IUST
Iran University of Science and Technology

Iranian Journal of Electrical and Electronic Engineering

Journal Homepage: ijeee.iust.ac.ir

Research Paper

Thrust Ripple Reduction of Permanent Magnet Linear Synchronous Motor Based on Improved Pole Shape for Electromagnetic Launcher System

H. Sheykhvazayefi*, S. R. Mousavi-Aghdam**(C.A.), and M. R. Feyzi*

Abstract: In this paper, a new design of permanent magnet linear synchronous motor (PMLSM) for electromagnetic launcher system (EMLs) has been investigated in terms of the requisite amount of average launching thrust force and thrust force ripple minimization through finite element method. EMLs are a kind of technology used to develop thrust force and launch heavy loads with different applications including military, aerospace, and civil applications. A linear motor as a major part of the system plays a substantial role in this application providing sufficient load launch force. Cogging force and its mitigation techniques are principle challenges in linear motor operation leading to thrust ripples and detrimental effects on positioning precision and dynamic performance of the moving part. In the proposed design, some modifications have been made in the conventional PMLSM structure. Semi-closed slot construction is used for the primary and the pole shoes width has been changed to access minimum thrust ripple value. In order to attain further optimization in PMLSM's thrust ripple profile, some other modifications have been considered in PM's shape as arc-shaped magnetic poles. The latter assists to enforce air gap flux density distribution as sinusoidal as possible, and makes further ripple reduction. The results exhibit that the proposed structure has low weight and it is more economical compared to conventional PMLSM with rectangular shape magnet. In addition, the Average thrust force and ripple are improved providing suitable thrust force for throwing the load.

Keywords: Linear Motor, Electromagnetic Launcher, Finite Element Method, Thrust Force Ripple.

1 Introduction

TO select a drive for EMLs application, there are two choices including linear induction motor and PMLSM. The linear induction machine with nonmagnetic secondary has a high magnetizing current and low power factor because of large air gap [1]. It needs high power inverter for supplying. On the other side, PMLSM does not have these drawbacks but needs expensive rare earth permanent magnets and some problems in permanent magnet demagnetization [2-4]. Due to their high efficiency, compact and simple mechanical structure, high thrust-to-current ratio, fast dynamic response, high power density, and easy maintenance and controllability [5-6], PMLSMs are appropriate for electromagnetic launcher systems. Additionally, these advantages of PMLSMs in EML have enabled it to supplant the steam catapult system that has large and heavy structure, tendency to unnecessarily overstress the airframe and operate without feedback control with low efficiency [7-9].

Cogging force and its reduction methods are one of the principal challenges in the linear PM motors operation. The cogging force, caused by the attraction force between permanent magnets and stator, produces the thrust ripples and harmful effects on positioning precision and dynamic performance and should be

Iranian Journal of Electrical and Electronic Engineering, 2019.
Paper first received 05 February 2019, revised 01 April 2019, and accepted 12 April 2019.
* The authors are with the Department of Electrical Engineering, Tabriz University, Tabriz, Iran.
E-mails: h.vazayefi@gmail.com and feyzi@uma.ac.ir.
** The author is with the Department of Electrical Engineering, University of Mohaghegh Ardabili, Ardabil, Iran.
E-mail: R.mousaviaghdam@uma.ac.ir.
Corresponding Author: S. R. Mousavi-Aghdam.

minimized for linear motor precise and stable operation [10-12].

Up to now, different methods have been proposed for decrease of the motor thrust ripple in order to enhance the PM motors efficiency. A method in [12] is proposed in which proper phase set shift is adopted, and then the summation of each cogging force component can be decreased. As the adopted shift angle become larger, the phase current for each set differs from exact angle and position in this case leads to reduction in the thrust force. Moving node techniques by using optimization algorithm and considering PM's dimension and air gap length as optimization variables is another method which could not have impressive impact on thrust ripple reduction due to restricted range of varied design parameters in machine topology [13-15].

Slotless core of the PMLSM's structure as another approach is considered to have a lower thrust ripple compared with slotted types. However, the air-gap flux density of a slotless motor is lower than that of a slotted one. For the EML system, high thrust requirement absolutely has a crucial role. Therefore, it could not be a reasonable selection for the electromagnetic launcher purpose [16-18]. The modular stator structure, which can be obtained by considering flux gaps into every stator tooth, could mitigate the resultant cogging torque consequently the torque ripple will be reduced if the flux gap width is chosen properly [22]. Another technique uses restraining force of electromagnetic damping-spring system and tuned viscoelastic damper that offsets the ripple force to decrease the thrust ripple that could not be the rational method because high acceleration value and launching thrust force are required [20, 21].

The other method is the Modular PM Pole Technique. In this model, the pole consists of three or more magnet pieces with different types and specifications so that the central part of the pole experiences a more intensive magnetic field with respect to the pole ends. However, it has two drawbacks. One is complex magnetization system and procedure that is expensive and time consuming and the other is the use of PM material that is not fully utilized in the pole ends [22-25]. Divided PM poles and asymmetric PM poles has also been presented in some literature. These methods suffer from reduction in the thrust force and non-uniform air gap, respectively. The last method is to use the Halbach magnetized topology. This method needs many magnet pieces with different size and direction of magnetization. Thus, it uses excessive amount of PM material, leading to a high production cost.

In this paper, a new design of PMLSM has been introduced and its performance is examined by finite element method in terms of the average thrust force and thrust force ripple. In proposed structures, the semi-closed slot construction has been used for primary structure of PMLSM. Moreover, the width of optimum pole shoe has been investigated to access minimum ripple. In order to establish a sinusoidal distribution of the air gap flux density, the arc-shaped magnetic poles are used in the secondary part of the PMLSM. Considering enough thrust force for the launcher, the motor radius and arc angle of permanent magnet are optimized to minimize the ripple.

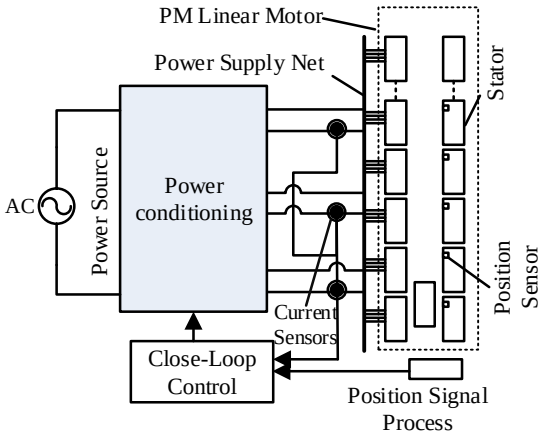

Fig. 1 Components of the electromagnetic launcher [26].

2 Electromagnetic Launcher System

Electromagnetic catapults are comprised of power source, power conditioning, launch motor, and closed-loop control subsystems all are shown in Fig. 1.

The applied power to the power conditioning subsystem is converted into a variant-frequency, variant-voltage power for supplying the linear motor. The linear motor, which is the main part of electromagnetic launchers, produces high thrust force to accelerate the shuttle along the launch route until the purposed weight can be thrown. The motors used in the electromagnetic catapult systems are linear induction motors or linear permanent magnet motors. Permanent magnet linear motors are more popular due to high power factor and do not need high power inverter to supply. The position sensors for closed-loop control are used in primary segments in order to determine the location of mover to supply just the windings that is involved at the time. The current sensors are also used in the closed-loop control to obtain the primary current in order to send controlling signals to the power conditioning [26-27].

If a typical launch of an object using electromagnetic launcher is considered, a mass of m has to be accelerated from 0m/s to a final velocity v_f m/s along the length l_f of the launch track by applying the linear motor force (F). Therefore, the mechanical system can be modeled as follows [2, 26, 28]:

$$F = \frac{mv_f^2}{2\ell_f} \tag{1}$$

$$a = \frac{v_f^2}{2\ell_f} \tag{2}$$

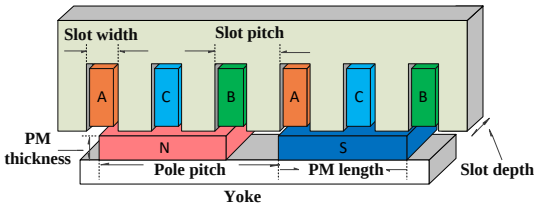

Fig. 2 Illustration of the single-sided conventional PMLSM with a pair of PMs.

$$\Delta t = \frac{2\ell_f}{v_f} \tag{3}$$

where F is the motor repulsion force, a is a constant acceleration and Δt is the launch time.

3 PMLSM Design for Launcher System

A double-sided PMLSM with blade shuttle structure is studied in this paper. The main dimensions and specifications of the motor are listed in Table 1. For simplicity, a schematic of single-sided structure of the motor with a pair of PMs is shown in Fig. 2.

Considering the double-sided structure of the PMLSM and its symmetry relative to the x-axis, all dimensions and components of the produced force at one edge are identical with the same values at the other edge. The horizontal force components of both edges are in the same direction (direction of projectile motion). The sum of these components determines thrust force of the linear motor. In return step, the vertical force components of each edge are in opposite direction of each other. The components of the opposing force ideally neutralize each other and prevent the moving part from deviating to one side and an asymmetrical occurrence in the air gap.

3.1 Design of Magnetic Circuit

Due to the different magnetizing directions of permanent magnet poles on both edges of the linear synchronous motor, there are two types of magnetic circuit include of the series and parallel magnetic circuits as shown in Fig. 3 [29]. In this paper, the series magnetic circuit is applied for the proposed motor because of larger thrust force and smaller thrust ripple of this type.

3.2 Primary Structure and Winding Requirements

Considering a typical plane weight of 24×10^3kg which is launched along 100m length of the runway and must be speeded up from 0m/s to the final takeoff velocity 100m/s along with 2000kg of the maximum active secondary weight, the total thrust force of 1.3MN is required using (1). The primary side of the proposed motor has a slotted structure that the three-phase distributed winding with range of 18kA are applied to the stator slots to obtain the desired total thrust force.

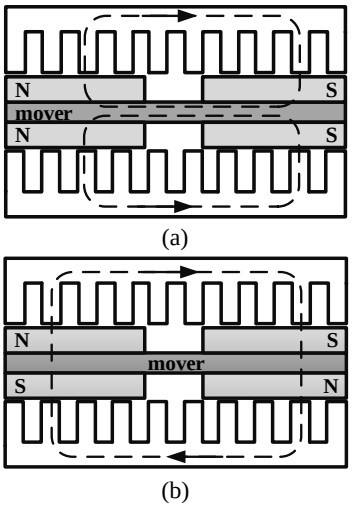

Fig. 3 Design of magnetic circuit. a) Parallel magnetic circuit, and b) Series magnetic circuit.

These conductors occupy a cross section of 15×40mm in each slot that only fills 60% of the slot's space. In this case, the current density in each slot should be 30A/mm^2. This leads to the total copper losses of 2MW for the whole launcher system. The motor power is typically considered as 60MW then the copper losses represent only 4% of the input power.

It should be mentioned that the launching process lasts approximately two seconds. In addition, the vertical component of magnetic flux density in the magnets with 18kA current is never below 0.4T in the direction of magnetization [8]. Considering magnetic characteristics of the permanent magnet utilized in this paper, it can be mentioned that the intrinsic coercive force of the magnet is greater than 1600kA/m at 100°C (working magnet temperature) and the remnant magnetic-flux density at 20°C is 1.15T. Whilst the permanent magnets experience maximum amount of demagnetization (614kA/m), this will not be an issue.

The currents of primary winding with the frequency of f produce a synchronous traveling magnetic field. The relationship between the synchronous velocity of the moving part of the launcher and frequency is as follows

$$v = 2f\tau \tag{4}$$

where τ and v are defined as the pole pitch and synchronous velocity of the moving part respectively [30].

Geometry parameters of the PMLSM design are shown in Fig. 2 and summarized in Table 1. Considering 150mm for pole pitch length as in (4), the current of distributed winding in primary slots will be able to produce a magnetic field with the frequency of 333Hz in the primary. It can move at the speed of 100m/s along the primary structure of the motor in direction of the shuttle's displacement.

Table 1 Design specifications of the PMLSM.

Parameter	Sign	Value [unit]
Pole pitch	τ	150 [mm]
Slot pitch	τ_s	50 [mm]
PM length	w_m	100 [mm]
Slot width	w_s	20 [mm]
Slot depth	h_s	50 [mm]
PM thickness	h_m	80 [mm]
Air gap length	g	8 [mm]
Slot current	I_m	18 [kA]

3.3 Shuttle Configuration

The structures used in the electromagnetic launcher shuttle consist of two types of blades and inverted *U* shuttle, as shown in Fig. 4. In the inverted *U* structure, the shuttle covers a central primary structure with two rows of permanent magnets while in the blade structure the shuttle is placed between two lateral stationary parts. The blade structure allows the lightest possible shuttle which is more appropriate for EMLS application. The double-sided stator also has very good thermal paths.

For the pole pitch of 150mm, a 3m shuttle length would involve 20 poles of Neodymium Iron Boron (NdFeB) magnets supported in a composite structure of the secondary. In order to withstand high stress on PMs by demagnetization effect and high amount of acceleration in linear motors, some special mechanical supports and structures are used which include special metalworking process to harness the PMs. Having gone through some tension experimental tests to evaluate PMs' durability under predicted circumstances, permanent magnet materials are formed accurately to place in desired position and are fixed with mechanical connection.

The magnet thickness is determined by two factors. One is the minimum feasible air gap and the design requirements for approximately 0.9T in the air gap. The second is the PM demagnetization characteristics for a slot current of 18kA. The proposed design uses an 8mm air gap on each side, and a total magnet thickness of 80mm. Considering 120mm for magnet widths, the total magnet mass for the shuttle computes to 1184kg.

4 The Proposed Structures

As already mentioned, the linear motor's thrust ripple has a decisive role in its operation specially applied fluctuation to the shuttle which may cause to drastic damage to the launched weight. The force ripple of the linear synchronous motor is due to the cogging force which is practically resulted by the counteraction between the permanent magnets and slotted primary structure. Therefore, in this paper, some proposed structures to decline the PMLSM's thrust ripple have been developed. In the proposed structures, the pole shoe configuration is used for primary core to achieve semi-closed primary structure shown in Fig. 5. The Semi-closed primary structure aims to reduce the reaction between the PMs and the stator core. In addition, the total thrust ripple of the motor can be cut down.

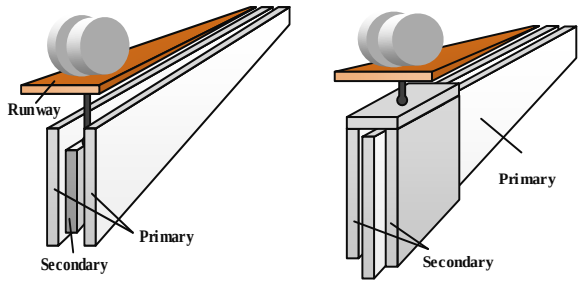

Fig. 4 Shuttle configuration: a) Blade shuttle, and b) Inverted U shuttle.

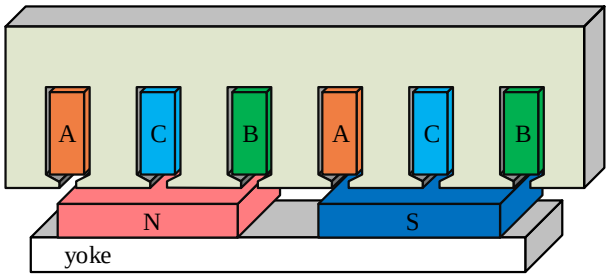

Fig. 5 The single-sided proposed semi-closed PMLSM with a pair of PMs.

The impact of multiple pole shoe width (from 0 mm for open slot to 9mm for closed slot) on average thrust and thrust ripple have been studied by using sensitivity analysis with respect to adequate throwing force attainment and least attainable thrust ripple.

By implementing different structure of the PMs as a step shaped PM in secondary framework of the PMLSM, the air gap flux density distribution will be closer to the sinusoidal waveform and the interaction between the slotted structure of the primary and permanent magnets will be minimized. Increasing the number of PM's steps makes the surface configuration of permanent magnets closer to the arc shape and also makes air gap flux density distribution so close to a sinusoidal waveform. Therefore, the second proposed structure which is called the arc-shaped PM is proposed in this analysis. Low cogging force of the arc-shaped structure prompts the total thrust ripple of the motor to diminish impressively and the motor control capability can be increased.

The curvature rate and the width of the arc-shaped permanent magnet are determined by the parameters of the arc radius (R) and the angle of the PM (α) according to Fig. 6(a). In this structure, the thrust force and ripple of the simulated motor have been investigated for various range of the mentioned parameters and desired values of R and α have been determined through sensitivity analysis to obtain the minimum thrust ripple.

Considering 40mm thickness of the permanent magnets, the single-sided arc shaped PMLSM with one pair of PM has been simulated for different values of the

Table 2 Parameters of R and alpha (symbol) for different width of arc-shaped permanent magnet..

w_m = 100mm		w_m = 105mm		w_m = 110mm		w_m = 115mm	
R [mm]	*α* [degree]	*R* [mm]	*α* [degree]	*R* [mm]	*α* [degree]	*R* [mm]	*α* [degree]
73	86.66	73	91.98	73	97.77	73	103.9
83	74.126	83	78.48	83	83.15	83	87.7
93	65.056	93	68.76	93	72.5	93	76.37
103	58.11	103	61.3	103	64.6	103	67.84
113	52.52	113	55.38	113	58.3	113	61.17
123	47.96	123	50.53	123	53.13	123	55.74

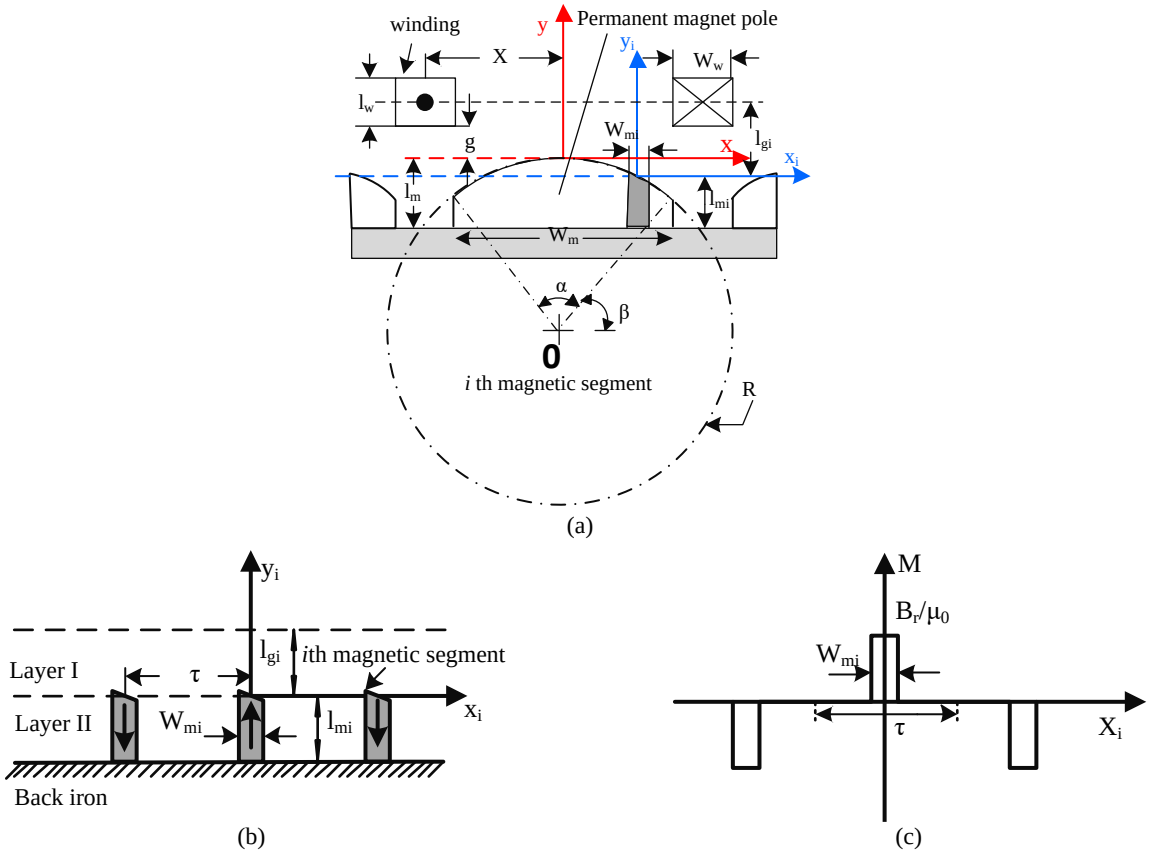

Fig. 6 Simplified model a) field regions, b) magnetization distribution c) of the machine.

parameters *R* and *α*. The width of the arc-shaped permanent magnets is specified by these parameters whose different quantities for various width ranges of the PM is presented in Table 2.

5 Analytical Model

In order to establish analytical solutions for the magnetic field distribution in the foregoing PMLSM, the length of the motor and permeability of the iron core are considered infinite as well as the PMs have linear demagnetization characteristic and their permeability is considered equal to the permeability of the free space.

Considering arc shapes of the magnets, solving of Maxwell equations for calculating magnetic field becomes more complex. Therefore, the solution of the field is approximated by dividing the PM into some finite different sectors as shown in Fig. 6(b). Assuming more segments for each PM, the height of given segment can be precisely approximated by a constant length as a rectangular shape segment. Thus, the layer model can be used to solve the Maxwell equations in each magnetic segment for the prediction of the field distribution. Consequently, the magnetic field analysis in terms of the *i*-th magnetic segment is enclosed to two regions, the airspace/winding and PM regions. Figs. 6(a) and 6(b) show simplified model of the machine topology and the field regions of the *i*-th segments. Therefore, the governing field equations in terms of the magnetic vector potential for the *i*-th segment lead to Laplace and Poisson equations as follows [31, 32]:

$$\begin{aligned} \nabla^2 A_{I_i} &= 0 && \text{in layer I} \\ \nabla^2 A_{II_i} &= -\mu_0 J_{M_i} && \text{in layer II} \end{aligned} \tag{5}$$

where M_i is the magnetization vector of the *i*-th magnetic segment.

The width of the *i*-th segment (W_{mi}) is obtained for the calculation of the magnetic potential vector along *y* axis as follows

$$W_{mi} = 2R\sin(\gamma_i)\sin\left(\frac{\alpha}{2j}\right) \quad (6)$$

where γ_i is a polar angle between the positive x-axis and an imaginary line dividing the α_i angle into two halves, and is given by

$$\gamma_i = \beta + (i-0.5)\frac{\alpha}{j} \quad (7)$$

The angles α and β displayed in Fig. 6(a) are expressed in terms of the following equation

$$\alpha = 2\sin^{-1}\left(\frac{w_m}{2R}\right) \quad (8)$$

$$\beta = \cos^{-1}\left(\frac{w_m}{2R}\right) \quad (9)$$

The boundary conditions to be satisfied are as follows

$$H_{Ix_i}\Big|_{y_i=l_{gi}} = 0, \qquad H_{IIx_i}\Big|_{y_i=-l_{mi}} = 0$$
$$H_{Ix_i}\Big|_{y_i=0} = H_{IIx_i}\Big|_{y_i=0}, \; B_{Iy_i}\Big|_{y_i=0} = B_{IIy_i}\Big|_{y_i=0} \quad (10)$$

where l_{mi} is the height of *i*-th segment, and l_{gi} is its effective air-gap length given by

$$l_{m_i} = l_m - R(1-\sin(\gamma_i)) \quad (11)$$

$$l_{g_i} = R(1-\sin(\gamma_i)) + g + l_w/2 \quad (12)$$

By solving (1), the normal components of the flux density produced by the *i*-th segment in the air gap are provided from the curl of A_{Ii} as follows

$$B_{Iy_i}(x_i, y_i) = \sum_{n=1,3,\ldots}^{\infty} m_n\left[a_{In_i}\cosh(m_n y_i) + b_{In_i}\sinh(m_n y_i)\right]\cos(m_n x_i) \quad (13)$$

where $m_n = n\pi/\tau$ and a_{In_i}, b_{In_i} are determined as

$$a_{In_i} = \frac{\left(e^{m_n l_{m_i}} - e^{-m_n l_{m_i}}\right)\left(e^{m_n l_{gi}} - e^{-m_n l_{gi}}\right)}{e^{m_n(l_{gi}+l_{mi})} - e^{-m_n(l_{gi}+l_{mi})}} \times\left(\frac{P_n\mu_0}{2m_n}\sin\left(\frac{m_n w_{m_i}}{2}\right)\right) \quad (14)$$

$$b_{In_i} = \frac{e^{-m_n l_{gi}} - e^{m_n l_{gi}}}{e^{m_n l_{gi}} + e^{-m_n l_{gi}}} \times a_{In_i} \quad (15)$$

The soft magnetic parts are assumed to be infinitely permeable and all materials behave linearly. Therefore, the resultant air-gap flux density is obtained in terms of *y* component by using the superposition theorem as

$$B_y(x,y) = \sum_{i=1}^{j} B_{Iy_i}\left[x + R\cos(\gamma_i)y - R(1-\sin(\gamma_i))\right] \quad (16)$$

The average thrust force exerted to the moving part is derived from winding current and fundamental component of flux density B_{y1} interaction produced by poles which is given as follow

$$F_{avg} = -\int J_z \times B_{y1}\,dv \quad (17)$$

Considering each coil of the primary winding which has been limited to $x_1 = x - w_w/2$, $x_2 = x + w_w/2$, $y_1 = g$, $y_2 = g + l_w$, the thrust force applied to the secondary can be obtained from the following formula

$$F_i(x_i) = 2\int_{x_i - l_w/2}^{x_i + l_w/2}\int_{R(1-\sin(\gamma_i))+g}^{R(1-\sin(\gamma_i))+g+l_w/2}\left(LJB_{y1}\right)dxdy \quad (18)$$

$$F_i(x_i) = K_i\sin(m_1 x_i) \quad (19)$$

$$K_i = 4LJp_f k_{w1}\sin\left(\frac{m_1 w_m}{2}\right) \times \int_{R(1-\sin(\gamma_i))+g}^{R(1-\sin(\gamma_i))+g+l_w/2}\left[a_{I1_i}\cosh(m_1 y_i) + b_{I1_i}\sinh(m_1 y_i)\right]dy \quad (20)$$

where *L* is motor width, p_f is coil packing factor and k_{w1} is winding factor of first harmonic. Therefore, the force F_{1ph_i} exerted to the secondary part from a phase winding is obtained using

$$F_{1ph_i}(x_i) = T_i\sin m_1\left(x_i - \frac{\tau_{wp}}{2}\right) \quad (21)$$

$$T_i = 2PK_i\cos\left(\frac{m_1\tau_{wp}}{2}\right) \quad (22)$$

where *P* is the number of pole pairs and τ_{wp} is winding pitch. Considering a three phase linear motor, the average thrust force implemented to the *i*-th segment of the PMs is obtained from

$$F_{3ph_i} = F_{A_i}(x_i) + F_{B_i}(x_i) + F_{C_i}(x_i) \quad (23)$$

$$F_{3ph_i} = \frac{3}{2}T_i\sin\left(\frac{\pi}{\tau}x_{0_i}\right) \quad (24)$$

In terms of all segments of the PMs, total average thrust force is given by [31, 32]:

$$F_{avg} = \sum_{i=1}^{j}\frac{3}{2}T_i\sin\left(\frac{\pi}{\tau}x_0 + R\cos(\gamma_i)\right) \quad (25)$$

where *R* is the magnet radius and x_0 is load angle.

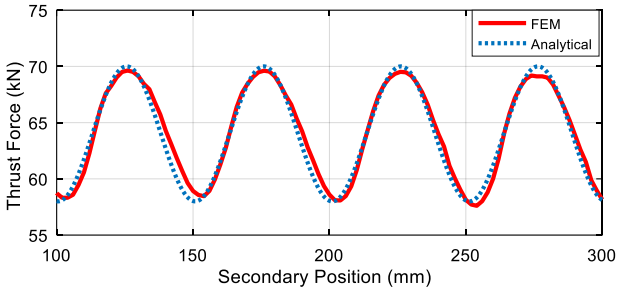

Fig. 7 Conventional PMLSM thrust force.

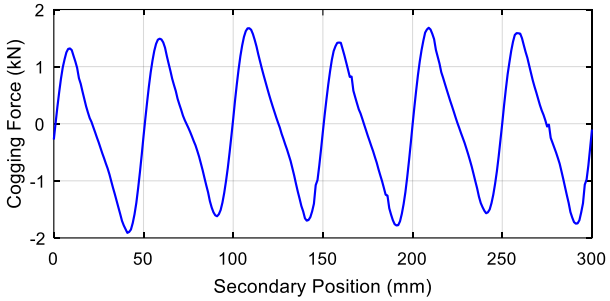

Fig. 8 Conventional PMLSM cogging force.

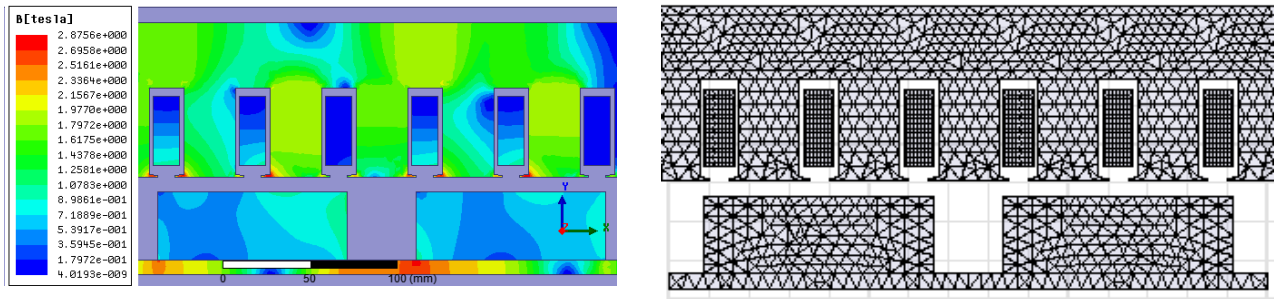

(a) (b)

Fig. 9 Finite element method results of the proposed PMLSM: a) Flux density distribution, and b) Mesh plot.

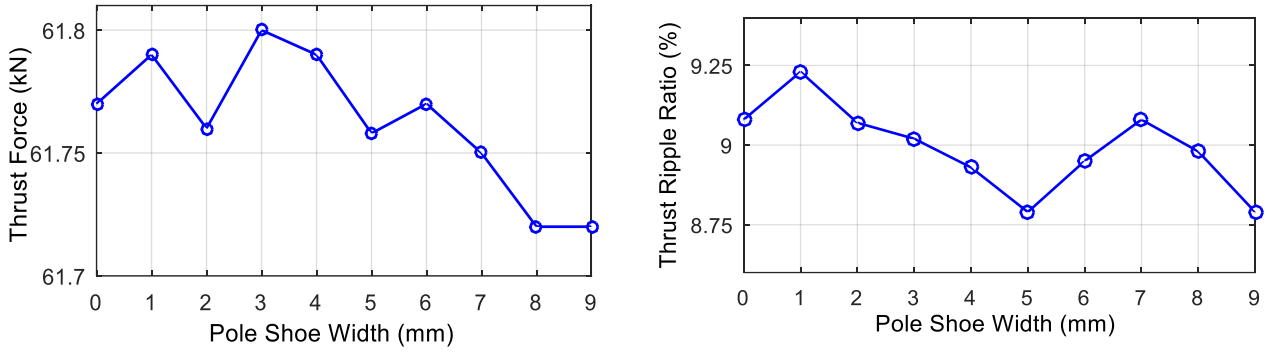

(a) (b)

Fig. 10 Results of the proposed semi-closed PMLSM in terms of pole shoe width: a) Average thrust force, and b) Thrust force ripple.

6 Simulation Results

In this paper, a single-sided conventional PMLSM (open slot with rectangular shaped PMs) with one pair of the PMs in secondary structure has been simulated based on the parameters in Table 1. Fig. 7 demonstrates generated thrust force of this motor in terms of shuttle position from 100mm to 300mm.

The average thrust force of the simulated single-sided conventional PMLSM with a pair of PM poles is 63.34kN. The same value is yielded 1.26MN for the double-sided PMLSM with 20 number of the moving part poles. This amount of the thrust force can be adequate in electromagnetic launcher purpose.

The cogging force of the simulated conventional PMLSM [8] has been displayed in Fig. 8. It can be observed that the peak to peak value of the linear motor's cogging force with open slot primary structure is 3.58kN whereas the total thrust ripple is remarkably declined by decrease of this value.

In the proposed semi-closed structure, whose flux density distribution and plotted mesh extended in Fig. 9, by utilizing pole shoe in the stator's teeth, the PMLSM's operation in electromagnetic launcher has been investigated in terms of thrust force and thrust force ripple profile. The appropriate pole shoe width has been obtained through sensitive analysis in order to provide sufficient thrust force and minimum thrust ripple along various amount of the parameter from 0mm (open slot structure) to 9mm. The results of the average thrust force for the single-sided proposed semi-closed PMLSM with two PMs and for different range of the pole shoe widths are indicated in Fig. 10 (a).

As shown in Fig. 10(b), for 5mm width of the pole shoe, the motor thrust ripple has its own minimum. Also, according to Fig. 10(a) the proposed semi-closed PMLSM would be able to meet the required thrust force of the electromagnetic launcher. Therefore, this value of

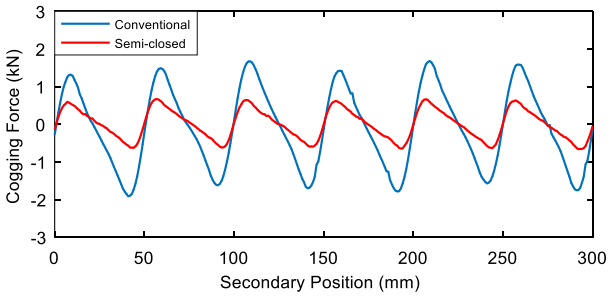

Fig. 11 The cogging force of the conventional and proposed semi-closed PMLSM.

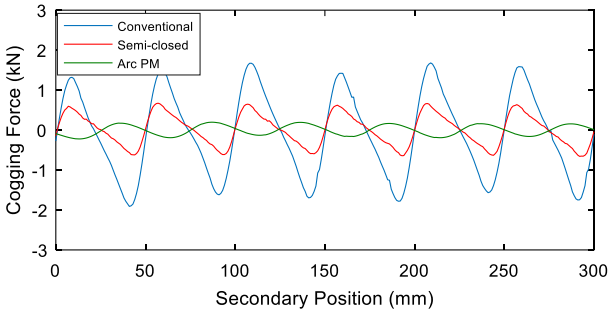

Fig. 12 The cogging force of the conventional PMLSM and proposed structures in terms of the PM width.

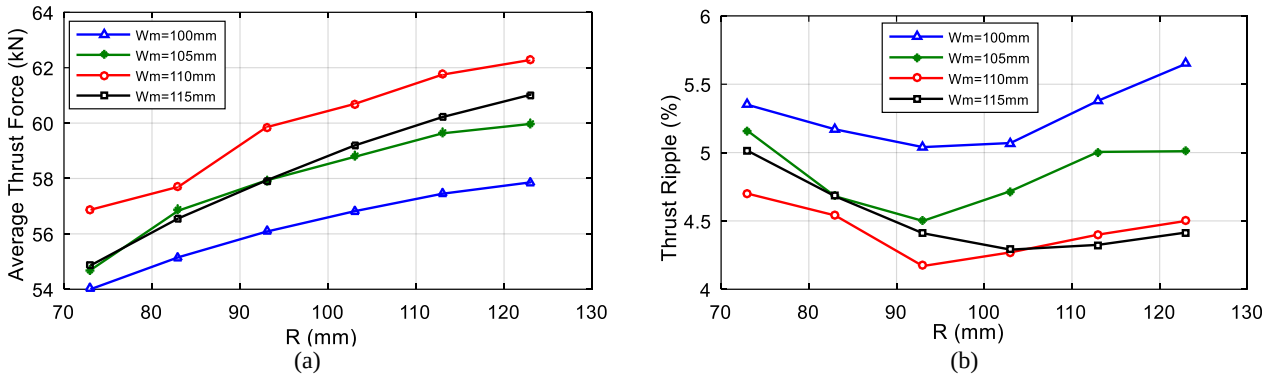

Fig. 13 Results of the proposed arc-shaped PMLSM in terms of arc radius: a) Average thrust force, and b) Thrust force ripple.

the pole shoe width is considered as the appropriate value of this parameter. After specifying the relevant amount of the pole shoe length, the cogging force of the conventional structure and proposed semi-closed (5mm width of the pole shoe) PMLSM are compared in Fig. 11.

According to Fig. 11, the peak to peak value of the proposed semi-closed PMLSM's cogging force are 1.33kN, whereas this values for conventional structure with open slot structure of the primary is 3.58kN. In this case, the total motor thrust ripple considering 100mm width of permanent magnets reduces from 12.9% for conventional structure to 8.58% for the proposed semi-closed structure. Therefore, the results exhibit that the thrust ripple value of the semi-closed structure is obviously lower.

It is expected that if rectangular PM is replaced with arc-shaped PM in secondary frame of the conventional PMLSM, the cogging force will be mitigated. Comparison between three different kinds of PMLSM including conventional PMLSM, proposed semi-closed PMLSM with rectangular PMs and proposed arc-shaped PMLSM with semi-closed slots have been carried out as shown in Fig. 12. It is obvious that the cogging force peak to peak value of the proposed arc-shaped PMLSM is 0.417kN and it is lower than that of the proposed semi-closed and conventional type respectively. In addition, cogging force of the arc-shaped PM's structure has the lowest average force among the others.

The average thrust force of the proposed arc-shaped PMLSM is indicated in terms of different width for various radius (R) of the secondary poles as in Fig. 13(a). As shown, the average thrust of the motor for 110mm width of the magnet (w_m=110mm) has the highest value than the other width of the permanent magnets. Now, the desired values of R, α and w_m can be determined by implementing sensitivity analysis to achieve minimum ripple and maximum average thrust force.

Fig. 13(b) shows the thrust ripple profile of the proposed arc-shaped PMLSM in terms of the parameter R and for different w_m values of the PM. The results exhibit that the proposed arc shaped structure with permanent magnet width of 110mm has lower thrust ripple than the others. Minimum thrust ripple of this motor takes place in R=93mm and α=72.5° with a 110mm width of PM, whose thrust force profile has been represented in Fig. 14. As a result, the ripple of 4.17% is achieved for proposed arc-shaped structure whereas the same value for the conventional PMLSM is 9.72%.

In electromagnetic launchers, since the thrust ripple in the steady state operation mode is very important in terms of the applied tension to the shuttle body and motor controllability enhancement. Therefore, the proposed arc shaped construction will be able to reduce the thrust ripple of the motor by 57.1% on the mode in comparison with the conventional PMLSM. The produced thrust forces of the conventional, proposed semi-closed and arc-shaped PMLSM are compared in Fig. 15.

According to Fig. 15 and Table 3, it can be realized

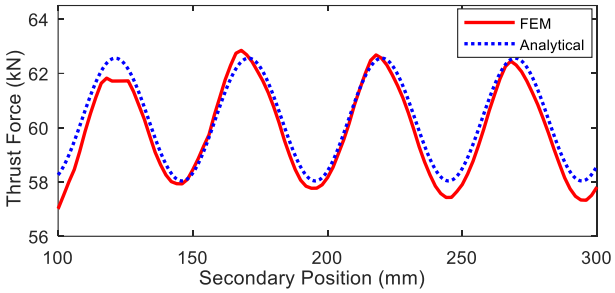

Fig. 14 Thrust force waveforms of proposed arc-shaped PMLSM in terms of secondary position.

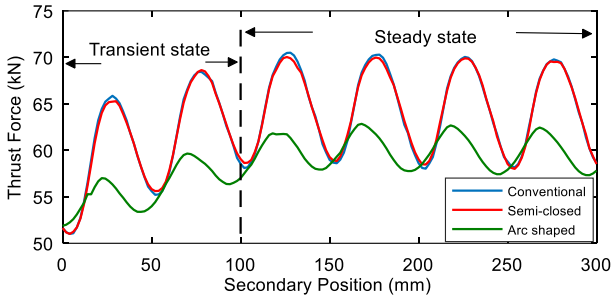

Fig. 15 Thrust force waveforms of conventional and proposed semi-closed and proposed arc-shaped PMLSM in terms of secondary position.

Table 3 Average trust force and trust ripple comparison of conventional PMLSM with rectangular PMs and proposed structures.

	Conventional PMLSM	Proposed semi-close PMLSM	Proposed arc-shaped PMLSM
Total thrust ripple	15.13	14.9	9.27
Steady state thrust ripple	9.72	9.03	4.17
Total average thrust (MN)	1.26	1.261	1.175

that the proposed arc-shaped PMLSM structures have lower thrust ripple than the conventional one with rectangular PMs. This improves the motor performance as well as increases its controllability. It is also observed that the proposed arc-shaped PMLSM has minimum thrust ripple value in both total and steady state operation mode. Although the total thrust force of the proposed arc-shaped structure is lower than the conventional type, this structure can be applied to PMLSMs just by small increase in lateral length of the motor up to 6.38%.

7 Conclusion

In this paper, a new design of PMLSM is introduced and its characteristics have been verified using the finite element method. Thrust force and thrust ripple profiles have been examined in order to supply adequate thrust value for launching purpose as well as minimum ripple amount of the linear motor thrust. Different structures have been proposed to oblige air gap flux density distribution closes to a sinusoidal waveform reducing interaction between slotted primary and permanent magnets including arc-shaped PMs and pole shoe implementation to the stator's teeth. As a result, considering the lowest thrust ripple, the optimal design of the motor has been achieved in order to enhance the capability of motor control and obtain minimum fluctuation to launched item's frame in electromagnetic launching system. The simulation results exhibit a better performance of the proposed design.

References

[1] M. Mirzaei, S. E. Abdollahi, and H. Lesani, "A large linear interior permanent magnet motor for electromagnetic launcher," *IEEE Transactions on Plasma Sciences*, Vol. 39, No. 6, pp. 1566–1570, 2011.

[2] M. Mirzaei, S. E. Abdollahi, and A. Vahedi, "Permanent magnet dc linear motor for aircraft electromagnetic launcher," in *14th Symposium on Electromagnetic Launch Technology*, Vancouver, BC, Canada, pp. 1–6, Jun. 2008.

[3] M. Mirzaei and S. E. Abdollahi, "Design optimization of reluctance synchronous linear machines for electromagnetic aircraft launch system," *IEEE Transactions on Magnetics*, Vol. 45, No. 1, pp. 389–395, 2009.

[4] G. Stumberger, D. Zarko, M. T. Aydemir, and T. A. Lipo, "Design and comparison of linear synchronous motor and linear induction motor for electromagnetic aircraft launch system," *IEEE International Electric Machines & Drives Conference (IEMDC'03)*, pp. 494–500, Jun. 2003.

[5] X. Wang, K. Cao, H. Feng, and L. Guo, X. Xu, "Design and analysis of permanent magnet linear synchronous motor with special pole shape," *Journal of Computers*, Vol. 8, No. 2, pp. 478–484, 2013.

[6] D. Y. Lee, and G. T. Kim, "Design of thrust ripple minimization by equivalent magnetizing current considering slot effect," *IEEE Transactions on Magnetics*, Vol. 42, No. 4, pp. 1367–1370, 2006.

[7] M. R. Doyle, D. J. Samuel, T. Conway, and R. R. Klimowski, "Electromagnetic aircraft launch system-EMALS," *IEEE Transactions on Magnetics*, Vol. 31, No. 1, pp. 528–533, 1995.

[8] D. Patterson, A. Monti, C. W. Brice, R. A. Dougal, R. O. Pettus, S. Dhulipala, D. C. Kovuri, and T. Bertoncelli, "Design and simulation of a permanent-magnet electromagnetic aircraft launcher," *IEEE Transactions on Industry Applications*, Vol. 41, No. 2, pp. 566–575, 2005.

[9] S. D. Grigorescu, A. Craciunescu, S. V. Paturca, L. Codreanu, H. Andrei, C. Cepisca, G. Seritan, O. M. Ghita, F. Argatu, "Coaxial linear motor for electromagnetic launchers," *The Scientific Bulletin of Electrical Engineering Faculty*, Vol. 1, No. ahead-of-print, 2016.

[10] Y. Yao, Y. Chen, Q. Lu, X. Huang, and Y. Ye, "Analysis of thrust ripple of permanent magnet linear synchronous motor with skewed PMs," in *18th International Conference on Electrical Machines and Systems (ICEMS)*, 25-28 Oct. 2015.

[11] M. J. Chung, M. G. Lee, S. Q. Lee, and S. M. Kim, "A method of optimal design for minimization of force ripple in linear brushless permanent magnet motor," in *Industry Applications Conference*, Vol. 1, pp. 36–39, Oct. 2000.

[12] J. Lim, and H. K. Jung, "Cogging force reduction in permanent magnet linear motor using phase set shift," in *18th International Conference on Electrical Machines*, pp. 1–4, Sep. 2008.

[13] L. Chunyan, and K. Baoquan, "Research on electromagnetic force of large thrust force PMLSM used in space electromagnetic launcher," *IEEE Transactions on Plasma Science*, Vol. 41, No. 5, pp. 1209–1213, 2013.

[14] K. C. Lim, J. K. Woo, G. H. Kang, J. P. Hong, and G. T. Kim, "Detent force minimization techniques in permanent magnet linear synchronous motors," *IEEE Transactions on Magnetics*, Vol. 38, No. 2, pp. 1157–1160, 2002.

[15] I. S. Jung, S. B. Yoon, J. H. Shim, and D. S. Hyun, "Analysis of forces in a short primary type and a short secondary type permanent magnet linear synchronous motor," *IEEE Transactions on Energy Conversion*, Vol. 14, No. 4, pp. 1265–1270, 1999.

[16] L. Li, M. Ma, B. Kou, and Q. Chen, "Analysis and optimization of slotless electromagnetic linear launcher for space use," *IEEE Transactions on Plasma Science*, Vol. 39, No. 1, pp. 127–132, 2011.

[17] A. H. Isfahani, "Analytical framepaper for thrust enhancement in permanent-magnet (PM) linear synchronous motors with segmented PM poles," *IEEE Transactions on Magnetics*, Vol. 46, No. 4, pp. 1116–1122, 2010.

[18] Y. S. Kwon, W. J. Kim, "Detent-force minimization of double-sided interior permanent-magnet flat linear brushless motor," *IEEE Transactions on Magnetics*, Vol. 52, No. 4, pp. 1–9, Apr. 2016.

[19] S. R. Mousavi-Aghdam, M. R. Feyzi, N. Bianchi, and M. Morandin, "Design and analysis of a novel high torque stator-segmented switched reluctance motor", *IEEE Transactions on Industrial Electronics*, Vol. 63, No. 3, pp. 1458–1466, 2016

[20] Z. He, F. Dong, J. Zhao, L. Wang, J. Song, and X. Song, "Thrust ripple reduction in permanent magnet synchronous linear motor based on electromagnetic damping-spring system," *IEEE Transactions on Energy Conversion*, Vol. 33, No. 4, pp. 2122–2132, Dec. 2018.

[21] Z. He, F. Dong, J. Zhao, L. Wang, J. Song, Q. Wang; and X. Song, "Thrust ripple reduction in permanent magnet synchronous linear motor based on tuned viscoelastic damper," *IEEE Transactions on Industrial Electronics*, Vol. 66, No.2, pp. 977–987, 03 May 2018.

[22] A. H. Isfahani, S. Vaez-Zadeh, and M. A. Rahman, "Using modular poles for shape optimization of flux density distribution in permanent magnet machines," *IEEE Transactions on Magnetics*, Vol. 44, No. 8, pp. 2009–2015, 2008.

[23] K. J. Meessen, B. L. J. Gysen, J. J. H. Paulides, and E. A. Lomonova, "Halbach permanent magnet shape selection for slotless tubular actuators," *IEEE Transactions on Magnetics*, Vol. 44, No. 11, pp. 4305–4308, 2008.

[24] J. S. Choi and J. Yoo, "Design of a Halbach magnet array based on optimization techniques," *IEEE Transactions on Magnetics*, Vol. 44, No. 10, pp. 2361–2366, 2008.

[25] M. Markovic and Y. Perriard, "Optimization design of a segmented Halbach permanent-magnet motor using an analytical model," *IEEE Transactions on Magnetics*, Vol. 45, No. 7, pp. 2955–2960, 2009.

[26] J. Lu and W. Ma, "Research on two types of linear machines for covert airstrip electromagnetic catapult," *IEEE Transactions on Plasma Science*, Vol. 39, No. 1, pp. 105–109, 2011.

[27] A. Musolino, R. Rizzo, and E. Tripodi, "The double-sided tubular linear induction motor and its possible use in the electromagnetic aircraft launch system," *IEEE Transactions on Plasma Science*, Vol. 41, No. 5, pp. 1193–1200, 2013.

[28] J. R. Quesada and J. F. Charpentier, "Finite difference study of unconventional structures of permanent-magnet linear machines for electromagnetic aircraft launch system," *IEEE. Transactions on Magnetics*, Vol. 41, No. 1, pp. 478–483, 2005.

[29] L. Li, M. Ma, B. Kou, and Q. Chen, "Analysis and design of moving-magnet-type linear synchronous motor for electromagnetic launch system," *IEEE Transactions on Plasma Science*, Vol. 39, No. 1, pp. 121–126, 2011.

[30] B. Reck, "First design study of an electrical catapult for unmanned air vehicles in the several hundred kilogram rang," *IEEE Transactions on Magnetics*, Vol. 39, No. 1, pp. 310–313, 2003.

[31] N. R. Tavana, A. Shoulaie, and V. Dinavahi, "Analytical modeling and design optimization of linear synchronous motor with stair-step-shaped magnetic poles for electromagnetic launch applications," *IEEE Transactions on Plasma Science*, Vol. 40, No. 2, pp. 519–527, Feb. 2012.

[32] N. R. Tavana, and A. Shoulaie, "Analysis and design of magnetic pole shape in linear permanent-magnet machine," *IEEE Transactions on Magnetics*, Vol. 46, No. 4, pp. 1000–1006, Apr. 2010.

H. Sheykhvazayefi was born in Ardabil, Iran, in 1987. He received the B.Sc. degree in Electrical Engineering from The University of Urmia, West Azerbaijan, Urmia in 2010 and the M.Sc. degree in Electrical Power Engineering (electric machines and drive) from the Tabriz University, Tabriz, Iran, in 2013. His research interests include design and modelling of electrical machines, finite-element analysis of electromagnetic devices and motor drives.

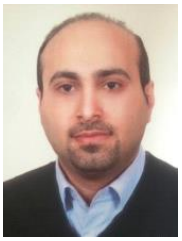

S. R. Mousavi-Aghdam received his B.Sc. degree with first class honor from Azarbaijan University of Shahid Madani in 2009, Tabriz, Iran, and M.Sc. and Ph.D. degree from University of Tabriz, Iran, in 2011 and 2015, respectively all in Electrical Engineering. During September 2014 to March 2015, he has been a Visiting Research Scholar at the Department of Industrial Engineering, University of Padova, Italy. Since 2016, he has joined the Department of Electrical Engineering, University of Mohaghegh Ardabili, Ardabil, Iran, as an Assistant Professor. His current research interests include design of electrical machines, electric drives and analysis of special electrical machines.

M. R. Feyzi received his B.Sc. and M.Sc. in 1975 from the University of Tabriz in Iran with honor degree. He worked in the same university during 1975 to 1993. He started his Ph.D. work at the University of Adelaide, Australia in 1993. Soon after his graduation, he rejoined to the University of Tabriz. Currently, he is a professor in the same university. His research interests are finite element analysis, design and simulation of electrical machines and transformers.

© 2019 by the authors. Licensee IUST, Tehran, Iran. This article is an open access article distributed under the terms and conditions of the Creative Commons Attribution-NonCommercial 4.0 International (CC BY-NC 4.0) license (https://creativecommons.org/licenses/by-nc/4.0/).